Published in final edited form as:
Magn Reson Med. 2008 June ; 59(6): 1378–1385. doi:10.1002/mrm.21617.

Respiratory Self-Gated Four-Dimensional Coronary MR Angiography: A Feasibility Study

Peng Lai[1,2], **Andrew C. Larson**[1], **Jaeseok Park**[1,2], **James C. Carr**[1], and **Debiao Li**[1,2,*]

[1] Department of Radiology, Northwestern University, Chicago, Illinois

[2] Department of Biomedical Engineering, Northwestern University, Chicago, Illinois

Abstract

The four-dimensional (4D) coronary MR angiography (MRA) approach has been developed to eliminate the need for accurate determination of the acquisition window and trigger delay time. Diaphragm navigator (NAV) has been the conventional respiratory gating method for free-breathing coronary MRA. However, NAV echo acquisition interrupts the continuous radiofrequency pulse application required for 4D steady-state free precession coronary MRA. The objective of this work was to investigate the feasibility of a respiratory self-gating (RSG) technique for 4D coronary MRA and its effectiveness by comparing with retrospective NAV gating. Data were acquired continuously throughout the cardiac cycle and retrospectively remapped to cardiac phases based on the electrocardiogram signal simultaneously recorded. An RSG signal extracted from a direct measurement of the heart position was used for retrospective respiratory gating and motion correction. In seven healthy volunteers, 4D MRA images were reconstructed, allowing retrospective assessment of the cardiac motion of the coronary artery and selection of the images with the best vessel delineation. Statistical analysis shows that 4D RSG provides coronary artery delineation comparable to mid-diastole images acquired using NAV. Respiratory self-gating is an effective method for eliminating respiratory motion artifacts and allows 4D coronary MRA during free breathing.

Keywords

coronary vessels; MR angiography; respiratory gating; motion correction

Overcoming cardiac and respiratory motion artifacts remains to be the major challenge in coronary MR angiography (MRA). Segmented data acquisition in combination with electrocardiogram (ECG) triggering is the conventional method to suppress cardiac motion artifacts. This method is intended to synchronize data acquisition with the period of minimal cardiac motion, usually the mid-diastole. Empirical formulas have been proposed to estimate the trigger delay time for mid-diastole (1,2). However, a cine scout scan and motion evaluation are usually required to accurately determine the trigger delay and acquisition window duration (3), because the optimal acquisition time not only varies among subjects, but also depends on the particular segment of the coronary artery being evaluated (4,5). Alternatively, cardiac motion-resolved (four-dimensional, 4D) coronary MRA was recently introduced to deal with the cardiac motion effect (6,7). With 4D data acquisition, coronary artery image sets throughout the cardiac cycle are reconstructed and the best delineation of coronary arteries can be selected retrospectively. However, resolving respiratory motion during cine data acquisition is thereby necessitated for high spatiotemporal-resolution 4D coronary MRA.

*Correspondence to: Debiao Li, Suite 1600, 737 North Michigan Avenue, Chicago, IL 60611. d-li2@northwestern.edu.

To suppress respiration-induced motion artifacts, various respiratory gating and correction methods have been developed (8–13). Among them, diaphragm navigator (NAV) is the most commonly used method for free-breathing coronary MRA (12,13). However, acquiring NAV echo before 4D coronary MRA acquisition at each cardiac phase will interrupt steady-state magnetization, resulting in potential image artifacts. Therefore, NAV has limited compatibility with 4D coronary MRA.

A few respiratory self-gating (RSG) schemes were recently proposed for cardiac or coronary artery imaging (14–16). Spiral or radial *k*-space sampling was used and data acquisition was interleaved such that a low-resolution two-dimensional (2D) image was reconstructed from each interleaf of *k*-space data. Information concerning the position of the heart can be extracted from the low-resolution image data for respiratory gating. With direct measurement of the heart position, the accuracy of respiratory synchronization and motion correction is expected to improve as compared to NAV techniques. However, with current MR imaging technology, it is impractical to achieve a sufficiently high sampling rate of three-dimensional (3D) low-resolution images for accurate respiratory gating signal derivation. Therefore, these interleaved *k*-space strategies are currently limited to 2D imaging.

Alternatively, Larson et al. (17) proposed a radial sampling-based self-gating method for tracking motion of the heart. Each radial *k*-space line was used to reconstruct a projection of the heart to derive the heart motion information for cardiac gating in cine imaging. Stehning et al. (18) used a similar method for respiratory gating in whole-heart coronary MRA. The respiration-induced bulk heart motion in the superior–inferior (SI) direction was estimated by calculating the shift of the center of mass of a SI projection derived from a center *k*-space line acquired before each segmented data acquisition.

The purpose of this work was to investigate the feasibility of acquiring 4D coronary MRA with RSG. A one-dimensional (1D) projection profile signal is acquired before each cardiac phase to track respiratory motion of the heart and is used for both retrospective respiratory gating and motion correction. Healthy volunteer studies were performed to demonstrate the effectiveness of the method in reducing respiratory motion artifacts by comparing with mid-diastole images acquired using retrospective NAV gating.

THEORY

In this work, an RSG *k*-space line is obtained before each cardiac phase by acquiring the center *k*-space line of the imaging volume, from which an RSG projection can be reconstructed using an inverse Fourier transform. According to the central section theorem of Fourier transform, the RSG projection, $P(x)$, represents the line-integral of the entire imaging volume along the phase-encoding (PE) direction, where x is the frequency-encoding (Freq) direction. For coronary MRA, because the target, defined as the region of the heart in the imaging volume, is not static due to respiratory and cardiac motion, $P(x)$ varies when repeatedly measured. Previous studies have shown that respiratory motion of the heart is dominated by a global 1D translation in the SI direction (19,20). Therefore, if Freq is in the SI direction, respiratory motion of the target is captured by the variation of $P(x)$. Two methods, Center of Mass (CM) and Least Squares (LS), were considered for deriving the breathing-induced displacement of the target from $P(x,t)$, the repeated measurement of the RSG projection.

CM, calculated with Eq. [1], is a first-moment measurement of the target position.

$$C(t)=\frac{\int |P(x,t)|\cdot x dx}{\int |P(x,t)| dx} \quad [1]$$

Early reports have demonstrated that *C(t)*, the change of CM, is synchronized with cardiac and respiratory motion and at a single cardiac phase provides an estimation of the respiratory motion of the target (17,18). However, unavoidably the relatively stationary signal from the anterior chest wall is superimposed into the RSG projection and may impair the accuracy of the derived target displacement. Furthermore, the extent of this undesired effect is determined by the ratio of the target signal to the total signal of the imaging volume and consequently is subject-dependent and orientation-dependent.

The LS method is capable of deriving subpixel displacements by matching the profile of a RSG projection with the profile template (21). The deviation (*DEV(*Δx*)*) of an RSG projection from the template at a displacement value Δx is calculated according to Eq. [2], where *h(x)* represents the template projection. The Δx resulting in the minimum deviation value is taken as $\bar{D}(t)$, the estimated displacement of the target at time t.

$$\begin{cases} \bar{D}(t)=\arg\min_{\Delta x} DEV(\Delta x) \\ DEV(\Delta x)=\int (|P(x-\Delta x,t)|-|h(x)|)^2 dx \end{cases} \quad [2]$$

Without steep edges defined by the boundaries between high-signal blood and low signal myocardium, the projection profile of the chest wall signal is relatively smooth compared with that of the heart signal such that the profile of the target is outstanding in the RSG projection. Due to this geometrical property, the LS method, based on detecting the shift of the target profile, is not sensitive to the superimposed chest wall signal.

To assess the effects of the chest wall signal on target displacement estimation, simulations were performed using a sagittal MR image through the left ventricle. The projection of the target and the projection of the anterior chest wall were simulated by integrating the complex signals along the anterior–posterior direction in the manually selected regions of the heart and the anterior chest wall in the image, respectively. As shown in Figure 1a, the anterior chest wall signal is comparable to the heart signal in magnitude and thus can substantially affect the target displacement estimation using CM. On the other hand, apparently the profile of the chest wall projection is much smoother than that of the heart projection. To simulate respiratory motion, the target projection was artificially shifted by integral pixels in the SI direction and the corresponding target displacements were estimated using the above two methods. As clearly shown in Figure 1b, compared with the CM method which underestimates the actual target shift by a factor of 0.676, the LS method is approximately a one-to-one measurement of the respiratory motion. To achieve more accurate respiratory motion correction, the LS method was used to derive the RSG signal as will be described later.

METHODS

Human studies were conducted in seven healthy volunteers (five males and two females; age: 39 ± 9) using a 1.5 Tesla (T) Magnetom Avanto clinical MRI scanner (Siemens Medical Solutions, Inc., Erlangen, Germany). In accordance with our institutional review board, written consent was obtained from each volunteer before imaging. For each study, first the heart and the diaphragm were localized from a low-resolution scout scan with three orthogonal views.

Next, a double-oblique plane covering the right coronary artery (RCA) was determined. Then, 4D free-breathing coronary MRA was performed using the RSG acquisition scheme (described in the next paragraph). To investigate the efficacy of RSG, coronary imaging was also performed using retrospective NAV gating. For a fair comparison between them, 3D NAV and 4D RSG scans were performed in the same slice position with identical spatial resolution. For both scans, the volunteer was allowed to breathe freely and the total scan time was approximately 6 min depending on the heart rate of the subject under study. All data processing and image reconstruction were performed off-line using the MATLAB software package (The Mathworks, Inc., Natick, MA).

Data Acquisition

A 4D RSG sequence was implemented based on a 3D SSFP cine sequence with retrospective cardiac gating and Cartesian *k*-space sampling (22). An additional RSG *k*-space line (a center *k*-space line with zero PE and partition-encoding gradients) was acquired before data acquisition of each cardiac phase. Because the in-plane respiratory motion of the target presumably corresponds to the projection of SI heart motion in the imaging plane, the in-plane rotation angle of the imaging volume was fixed to zero to automatically orient the Freq direction parallel to the direction of maximum in-plane respiratory motion. Imaging parameters included: $320 \times 245\ mm^2$ field of view, 1.4 mm slice thickness, 12 partitions (interpolated from 6 partitions), 320×204 matrix size, $1.0 \times 1.2\ mm^2$ in-plane resolution, 12 lines/per cardiac cycle, 60° flip angle, TR\TE = 4.0\2.0 ms. The average cardiac cycle length of the volunteer was individually estimated from the detected ECG signal before the 4D RSG scan. To resolve respiratory motion, each segmented data acquisition (1 RSG *k*-space line and 12 imaging *k*-space lines) was repeated for an acquisition window approximately covering four consecutive heartbeats.

Image Reconstruction

Data acquisition was synchronized with cardiac motion retrospectively using the simultaneously recorded ECG time stamps (23), indicating the time interval between the acquisition of a *k*-space line and the latest R-wave detection. Each *k*-space line was linearly remapped into the nearest cardiac phase of 15 evenly spaced phases based on the ratio of its time stamp to the duration of the corresponding cardiac cycle. Next, an RSG signal representative of the breathing-induced heart displacement was derived from the RSG projections to perform retrospective respiratory gating and motion correction. The reconstruction procedure consisted of three major steps: (i) generation of cardiac phase-specific profile templates, (ii) derivation of the RSG signal, and (iii) retrospective respiratory gating and motion correction.

Step 1: Generation of Cardiac Phase-Specific Profile Templates—Using the LS method, the displacement of the target along the Freq direction can be estimated by matching the profile of the RSG projection with the profile of the projection template. Because of both cardiac and respiratory motion, the profile of the RSG projection changes substantially during a scan. As shown in Figure 2a, the RSG projections acquired at end-expiration show dramatically different profiles at mid-systole (dotted line) and mid-diastole (solid line). In Figure 2b, distortions in addition to a global shift of the RSG projection are observed when comparing an end-inspiration profile (dashed line) to an end-expiration profile (solid line) at the same cardiac phase. The profile distortion at different respiratory phases can be attributed to nonrigid motion of the heart and through-plane motion in free-breathing volume-targeted imaging. To accurately estimate the global shift of the RSG projection during breathing, profile distortions due to cardiac and respiratory motion need to be eliminated. Cardiac motion effects can be suppressed by generating a profile template for each cardiac phase. As shown in Figure 3, the significant cardiac-motion modulations of the target shifts derived using single-phase

profile matching (Fig. 3a) were substantially reduced by using cardiac phase-specific profile matching (Fig. 3b). To minimize the effects of breathing-related profile distortions, the profile template at an end-expiration position near which data are accepted for image reconstruction should be used. The CM method was used to determine the reference respiratory position, because, although inaccurate quantitatively, CM is synchronized with respiratory motion at each cardiac phase and can be directly calculated from the RSG projections. Specifically, the CM of each RSG projection acquired during the first 30 sec was calculated and the respiratory position corresponding to the most superior CM value at each cardiac phase was identified as the reference end-expiration position for that cardiac phase at which the profile template was calculated. Heart rate variations during a scan may cause mismapping of the selected profile templates with the cardiac phases and result in artifacts in the derived profile shift signal. To reduce these artifacts, at each cardiac phase, the profile template was generated by averaging the first five RSG projections acquired at the reference end-expiration position.

Step 2: Derivation of the RSG Signal—Profile shift in the RSG projection was derived using the LS method. To reduce the contamination of the signal from surrounding structures, profile matching was confined in the region of the heart in the RSG projections which was defined manually in the profile templates.

The profile-shift signal derived hereby is an estimation of the in-plane respiratory motion of the heart with residual cardiac motion modulation as well as high-frequency noise. In a normal subject, respiratory motion is of relatively low frequency (<0.4Hz), while cardiac motion is of relatively high frequency (0.8–1.5 Hz). Therefore, the profile-shift signal was low-pass filtered (pass frequency of 0.5 Hz and cut-off frequency of 0.6 Hz) to obtain an RSG signal representing the breathing-induced bulk displacement of the heart. The position with the maximum frequency of occurrence during the scan, normally near the end-expiration, was then chosen as the RSG position.

Step 3: Retrospective Respiratory Gating and Motion Correction—Adaptive averaging (described in the next paragraph) of measurements within the gating window (GW) was used to optimize signal-to-noise ratio (SNR). Generally, a choice of a wider GW includes more data in image reconstruction and, therefore, benefits SNR. However, this also introduces an increased risk of blurring due to breathing-induced heart deformation and through-plane motion. To be consistent with retrospective NAV gating using a fixed GW along the SI direction, the GW for 4D RSG was individually calculated based on the angle between the Freq direction and the SI direction. In the current work, a GW corresponding to the projection of ± 1.5 mm of SI heart motion (as will be used in NAV gating) in the Freq direction was used.

Respiratory gating was performed by selecting *k*-space segments with consistent target position retrospectively. The displacements of the two RSG projections acquired before and after a *k*-space segment were averaged to estimate the target displacement during acquisition of the *k*-space segment. Each *k*-space segment was repeatedly acquired for roughly four cardiac cycles and, therefore, was acquired multiple times at each cardiac phase. Among them, those with a displacement within the GW were accepted as consistent data. In the case that none of them was qualified for acceptance, the acquisition with the smallest displacement was accepted. According to the Fourier shift theorem, respiratory motion causes a linear phase modulation in *k*-space. This effect can be suppressed by applying an inverse phase modulation *M(k)* in the accepted *k*-space lines (Eq. [3]).

$$M(k)=\exp(i2\pi \cdot k \cdot \Delta x/N_x) \quad [3]$$

where Δx is the derived displacement of the target from the RSG position in the unit of pixel, k and N_x are the sample index (center k-space sample: $k = 0$) and the total number of samples in a k-space line, respectively. Subsequently, at each cardiac phase, all accepted samples in the same k-space point were averaged to fill the 4D k-space for image reconstruction.

Phase-Sensitive Fat Suppression

Signal from fat was suppressed using the phase-detection method (24) previously used for breath-hold 4D coronary MRA (7). Briefly, this method is capable of separating fat and water signals based upon the phase difference between fat and water signals in the complex images obtained using SSFP acquisition schemes (7,24). For these studies, local phase correction was applied in each block of 10 × 10 pixels and phase-corrected images were then used for fat/water separation according to the polarity of the real part of the signal in each pixel.

3D NAV

Before 3D NAV imaging, the optimal acquisition window in a cardiac cycle, presumably at mid-diastole, was estimated by identifying the interval with minimal RCA motion from a cine scout scan at a four-chamber orientation. The 3D coronary MRA was performed using the predetermined trigger delay using a conventional 3D SSFP sequence with retrospective NAV gating, T2-preparation, and spectrally selective fat-saturation pulses (13,25). The NAV beam was positioned through the right semi-diaphragmatic dome and a flip angle of 70° was used. Other imaging parameters were the same as those for the 4D RSG scan. Similar to the 4D RSG scan, the same data acquisition per heartbeat was repeated four times to approximately cover a respiratory cycle.

Diaphragmatic motion was derived from the repeatedly measured NAV echo using a conventional edge-detection method (13) and multiplied by 0.6 to estimate SI heart motion (19). Next, heart motion in the SI direction was projected to the three orthogonal axes of the imaging coordinate, namely, frequency-, phase-, and partition-encoding directions. In each cardiac cycle, motion compensation was performed in the imaging coordinate by multiplying k-space samples with an inverse phase modulation term, $M'(k)$ (Eq. [4]).

$$M'(k,l,m)=\exp\left(i2\pi\cdot\left(\frac{k\cdot\Delta x}{N_x}+\frac{l\cdot\Delta y}{N_y}+\frac{m\cdot\Delta z}{N_y}\right)\right) \quad [4]$$

where, k, l, and m represent the k-space indices in the frequency-, phase-, and partition-encoding directions, respectively. N_x, N_y, and N_z are the k-space matrix sizes in the frequency-, phase-, and partition-encoding directions, respectively. Δx, Δy, and Δz are the derived heart displacements in the unit of pixel in the frequency-, phase-, and partition-encoding directions, respectively. Subsequently, similar to RSG, the most consistent respiratory position was selected as the gating position and adaptive averaging was performed using a GW of ±2.5 mm (corresponding to ± 1.5 mm for SI heart motion).

Statistical Analysis of Image Quality

Images were reconstructed using both 4D RSG and 3D NAV gating and preliminary comparisons were made between them to assess the effectiveness of the RSG technique on eliminating respiratory motion artifacts. The mid-diastolic phase was individually identified by selecting the cardiac frame providing the best coronary artery depiction from 4D RSG image series. Maximum-intensity-projection (MIP) images from the seven volunteers were displayed in seven rows separately. In each row, the mid-diastole RSG image and the NAV image were placed side by side with their order of placement (right or left) randomized. These images were

independently scored by two experienced cardiac MRI specialists blinded to the reconstruction technique. A scoring system (0–4) was designed to evaluate the image quality based on coronary artery delineation: “0” indicates completely unintepretable image quality (coronary artery invisible); “1” indicates poor image quality (coronary artery visible, with markedly blurred edges); “2”indicates acceptable image quality (coronary artery visible, with moderately blurred edges); “3” indicates good image quality (coronary artery visible, with mildly blurred edges); “4”: indicates excellent image quality (coronary visible, with sharply defined edges).

The scores from the two reviewers were averaged as the overall qualitative evaluation of coronary vessel delineation for a given image. The image scores for 4D RSG and 3D NAV were compared using a Wilcoxon signed rank test with significance level of 0.05.

RESULTS

RSG Signal

Figure 4a shows a typical segment (~40 s) of the repeatedly acquired RSG projection. The region of the heart, shown as the region between the two white dotted lines, exhibits a characterized motion pattern consisting of a relatively slow respiratory motion component and a relatively fast cardiac motion component. The corresponding profile-shift signal of the target derived using the LS method is shown in Figure 4b, with residual cardiac motion modulations evident. After low-pass filtering, these cardiac-motion artifacts as well as high-frequency noise were suppressed to obtain a smooth RSG signal representing the breathing-induced displacement of the target (Fig. 4c). Consistency between the derived RSG signal and the respiratory motion of the target in Figure 4a can be clearly appreciated.

Based on the derived RSG signal, the histogram of target position during the scan was obtained and plotted in Figure 5. Target position was linearly mapped into indexes 1 to 20, with 1 for the lowest target position (end-inspiration) and 20 for the highest target position (end-expiration). The position with the highest frequency of occurrence (indicated by the solid bold line in Fig. 4c and the black bar in Fig. 5) was chosen as the RSG position.

Respiratory Gating and Adaptive Averaging

Figure 6 is a cine show of the MIP images acquired using 4D RSG. In-plane and through-plane motion of RCA throughout the entire cardiac cycle is clearly visualized in the multi-phase image series. The best vessel delineation was obtained in the mid-diastolic frame at cardiac phase 12 (Fig. 7a). Figure 7b shows the image acquired using NAV from the same volunteer. Similar coronary artery depiction was observed in these two images. However, a closer scrutiny reveals that the medial segment (black arrows) of RCA is visualized with sharper edges but exhibits slight signal drop in the RSG image as compared with the NAV image.

Figure 8 shows another example. With 4D imaging, cardiac motion of the coronary artery throughout the entire cardiac cycle is captured and contiguous phase images from early-diastole to late-diastole (Fig. 8e–g) can be visually assessed. Clearly, RCA is best visualized at cardiac phase 11 in this case. Noticeably, a distal segment (white arrows) of RCA indistinguishable at mid-diastole (Fig. 8f) is visualized in a late-systolic frame (Fig. 8d). Overall vessel delineation is comparable in the mid-diastole images acquired using 4D RSG (Fig. 8f) and 3D NAV (Fig. 8i).

Image Quality Analysis

The mean image quality scores from the two reviewers along with the averaged scores are shown in Table 1. On average, both reviewers graded the RSG images slightly higher than the NAV images. The difference between them is not statistically significant ($P > 0.05$).

DISCUSSION

Over the past decade, segmented data acquisition with NAV-gating and ECG-triggering has been successfully applied for free-breathing coronary MRA. In this study, we presented a new 4D RSG technique capable of resolving respiratory motion during cine imaging and yielding multi-phase image series characterizing cardiac motion of the coronary artery throughout the entire cardiac cycle.

An advantage of our method is that the respiratory gating data are acquired in the imaging volume without disturbing steady-state magnetization and remarkably affecting temporal resolution such that cardiac motion-resolved SSFP imaging can be performed. By selecting the images with the best vessel delineation, postsynchronization of data acquisition with the optimal acquisition time can be achieved. Thus, protocol set-up is simplified. Contrarily, time-resolved imaging with high spatial resolution is impractical with conventional breath-holding and NAV techniques, because of its requirements for long scan time and cine data acquisition.

Furthermore, the 4D RSG method is capable of real-time and direct measurement of heart position. Using the phase-specific profile matching method, an RSG signal representing the breathing-induced motion of the target can be derived. Up-to-date target position information can be obtained for each *k*-space segment from the two neighboring RSG projections (separated by approximately 50 ms) and used for respiratory gating and motion correction. In comparison, conventional NAV measures diaphragm motion and uses a fixed correlation factor of 0.6 to correct the heart motion based on the diaphragm position shift (26), while the correlation factor that best represents the relationship between the SI coronary motion and diaphragm motion is both subject-dependent and artery-dependent (27). An inaccurate correlation factor and the hysteretic property of the correlation can lead to residual image artifacts (26). Therefore, compared with the NAV, this RSG technique potentially is self-adapted to the individual subject under study and can lessen the time-delay problem existing in the NAV technique. Further quantitative evaluation is necessary to investigate the accuracy of this RSG method in heart position measurement.

In addition, as opposed to the original RSG methods discussed in the introduction (14–16), this new RSG strategy is compatible with 3D data acquisition and, therefore, more appropriate for high-definition coronary MRA. Moreover, the RSG signal derived in our work was extracted from 1D projections. Processing of 1D signals is far less computationally intensive than the reconstruction and processing of real-time 2D images as required by the previous RSG strategies (14–16). This feature is especially beneficial to on-line implementation and prospective gating.

These preliminary studies were conducted with volume-targeted imaging. Only the displacement in the imaging volume can be detected. Therefore, when scanning left coronary artery systems with more transverse orientations, the dominant SI respiratory motion is through-plane and can cause inaccurate respiratory motion detection. Moreover, as observed in our volunteer studies, the target coronary artery may move out of the imaging volume and thus cannot be visualized in some cardiac phases due to significant cardiac motion. This impedes capturing the motion of the coronary artery throughout the cardiac cycle. However, these limits in orientation and coverage are not intrinsic problems in this RSG technique. Future work should extend the RSG scheme to whole-heart coronary MRA, where the SI respiratory motion can be assessed based on RSG projections acquired in this direction (28) and the entire coronary artery system is imaged.

An underlying assumption in the 1D-projection-based RSG technique is that the respiratory motion of the heart can be approximately reduced to a 1D SI translation. In accordance with early investigations (19,20), this feature was observed in all of our volunteer studies: in-plane

respiratory motion of the target exhibited primarily 1D translation corresponding to the projection of the SI respiratory motion of the heart in the imaging plane. However, it must be noted that translations in the anterior–posterior and left–right directions as well as rotation and deformation may be sufficient to cause considerable motion artifacts, especially with a large GW (29). Therefore, similar to NAV, appropriate selection of GW is critical to suppression of motion artifacts as well as reduction of scan time. The value of this optimal GW is dependent on both the accuracy of this RSG method in approximating global heart translation and the severity of non–SI-translation motion components. Further experiments should be done to quantitatively evaluate these factors such that an empirically optimal GW can be determined for the RSG technique.

Another issue worth noting is that respiratory motion was resolved by retrospective gating in this work. However, such a repeated sampling scheme leads to great redundancy in data acquisition. Furthermore, retrospective gating cannot ensure acquisition of all necessary data at consistent respiratory positions and thus retain considerable respiratory motion artifacts (30). The relative low image quality due to retrospective gating as well as the incomplete motion detection for RSG with volume-targeted data acquisition may affect the comparison between RSG and NAV. Thus, future work should implement prospective RSG and perform a more complete comparison between these two techniques.

Additionally, fat saturation is a challenging issue for time-resolved SSFP imaging. We currently used a phase-detection method to separate fat signals from water signals. The major advantage of this method is it can be simply fitted to conventional cine SSFP imaging. However, this method is susceptible to partial-volume effects (24). Due to cancellation of oppositely phased fat spins and water spins in the same voxel, signal intensity at the edge of the coronary artery may be reduced and small branches of the coronary artery may not be visible. This effect may have contributed to the reduced signal intensity of the medial RCA in the 4D RSG image in Figure 7. Recently, Derbyshire et al. (31) proposed a new fat suppression technique, Spectrally Selective Suppression with SSFP, and reported promising results in real-time cardiac imaging. This approach can significantly attenuate fat signals without disturbing SSFP steady state and, therefore, should be a better solution to fat saturation in 4D coronary MRA.

In conclusion, with the volunteer studies, we have demonstrated the feasibility of using the new 4D RSG strategy for high-quality free-breathing time-resolved coronary MRA and preliminarily validated its effectiveness by comparing with retrospective NAV. Future work will implement real-time prospective RSG and quantitatively evaluate the accuracy of this technique for suppressing respiratory motion in comparison with conventional NAV techniques.

Acknowledgments

Grant sponsor: National Institutes of Health; Grant number: NIBIB EB002623; Grant number: NHLBI HL079148; Grant sponsor: Siemens Medical Solutions USA, Inc., Malvern, PA.

References

1. Weissler AM, Harris WS, Schoenfeld CD. Systolic time intervals in heart failure in man. Circulation 1968;37:149–159. [PubMed: 5640345]
2. Stuber M, Botnar RM, Danias PG, Kissinger KV, Manning WJ. Submillimeter three-dimensional coronary MR angiography with real-time navigator correction: comparison of navigator locations. Radiology 1999;212:579–587. [PubMed: 10429721]
3. Wang Y, Watts R, Mitchell I, Nguyen TD, Bezanson JW, Bergman GW, Prince MR. Coronary MR angiography: selection of acquisition window of minimal cardiac motion with electrocardiography-

triggered navigator cardiac motion prescanning—initial results. Radiology 2001;218:580–585. [PubMed: 11161182]

4. Wang Y, Vidan E, Bergman GW. Cardiac motion of coronary arteries: variability in the rest period and implications for coronary MR angiography. Radiology 1999;213:751–758. [PubMed: 10580949]
5. Johnson KR, Patel SJ, Whigham A, Hakim A, Pettigrew RI, Oshinski JN. Three-dimensional, time-resolved motion of the coronary arteries. J Cardiovasc Magn Reson 2004;6:663–673. [PubMed: 15347131]
6. Bi X, Park J, Larson AC, Zhang Q, Simonetti O, Li D. Contrast-enhanced 4D radial coronary artery imaging at 3.0 T within a single breath-hold. Magn Reson Med 2005;54:470–475. [PubMed: 16032681]
7. Park J, Larson AC, Zhang Q, Simonetti O, Li D. 4D radial coronary artery imaging within a single breath-hold: cine angiography with phase-sensitive fat suppression (CAPS). Magn Reson Med 2005;54:833–840. [PubMed: 16149060]
8. Edelman RR, Manning WJ, Burstein D, Paulin S. Coronary arteries: breath-hold MR angiography. Radiology 1991;181:641–643. [PubMed: 1947074]
9. Manning WJ, Li W, Edelman RR. A preliminary report comparing magnetic resonance coronary angiography with conventional angiography. N Engl J Med 1993;328:828–832. [PubMed: 8285929]
10. Wang Y, Grimm RC, Rossman PJ, Debbins JP, Riederer SJ, Ehman RL. 3D coronary MR angiography in multiple breath-holds using a respiratory feedback monitor. Magn Reson Med 1995;34:11–16. [PubMed: 7674888]
11. Bailes DR, Gilderdale DJ, Bydder GM, Collins AG, Firmin DN. Respiratory ordered phase encoding (ROPE): a method for reducing respiratory motion artefacts in MR imaging. J Comput Assist Tomogr 1985;9:835–838. [PubMed: 4019854]
12. Wang Y, Rossman PJ, Grimm RC, Riederer SJ, Ehman RL. Navigator-echo-based real-time respiratory gating and triggering for reduction of respiration effects in three-dimensional coronary MR angiography. Radiology 1996;198:55–60. [PubMed: 8539406]
13. Li D, Kaushikkar S, Haacke EM, Woodard PK, Dhawale PJ, Kroeker RM, Laub G, Kuginuki Y, Gutierrez FR. Coronary arteries: three-dimensional MR imaging with retrospective respiratory gating. Radiology 1996;201:857–863. [PubMed: 8939242]
14. Hardy CJ, Saranathan M, Zhu Y, Darrow RD. Coronary angiography by real-time MRI with adaptive averaging. Magn Reson Med 2000;44:940–946. [PubMed: 11108632]
15. Sussman MS, Stainsby JA, Robert N, Merchant N, Wright GA. Variable-density adaptive imaging for high-resolution coronary artery MRI. Magn Reson Med 2002;48:753–764. [PubMed: 12417989]
16. Larson AC, Kellman P, Arai A, Hirsch GA, McVeigh E, Li D, Simonetti OP. Preliminary investigation of respiratory self-gating for free-breathing segmented cine MRI. Magn Reson Med 2005;53:159–168. [PubMed: 15690515]
17. Larson AC, White RD, Laub G, McVeigh ER, Li D, Simonetti OP. Self-gated cardiac cine MRI. Magn Reson Med 2004;51:93–102. [PubMed: 14705049]
18. Stehning C, Bornert P, Nehrke K, Eggers H, Stuber M. Free-breathing whole-heart coronary MRA with 3D radial SSFP and self-navigated image reconstruction. Magn Reson Med 2005;54:476–480. [PubMed: 16032682]
19. Wang Y, Riederer SJ, Ehman RL. Respiratory motion of the heart: kinematics and the implications for the spatial resolution in coronary imaging. Magn Reson Med 1995;33:713–719. [PubMed: 7596276]
20. McLeish K, Hill DL, Atkinson D, Blackall JM, Razavi R. A study of the motion and deformation of the heart due to respiration. IEEE Trans Med Imaging 2002;21:1142–1150. [PubMed: 12564882]
21. Hajnal JV, Saeed N, Soar EJ, Oatridge A, Young IR, Bydder GM. A registration and interpolation procedure for subvoxel matching of serially acquired MR images. J Comput Assist Tomogr 1995;19:289–296. [PubMed: 7890857]
22. Lai, P.; Larson, A.; Park, J.; Carr, J.; Li, D. Respiratory self-gated 4D coronary MRA. Proceedings of the 14th Annual Meeting of ISMRM; Seattle, USA. 2006. p. 364
23. Glover GH, Pelc NJ. A rapid-gated cine MRI technique. Magn Reson Annu 1988:299–333. [PubMed: 3079300]

24. Hargreaves BA, Vasanawala SS, Nayak KS, Hu BS, Nishimura DG. Fat-suppressed steady-state free precession imaging using phase detection. Magn Reson Med 2003;50:210–213. [PubMed: 12815698]

25. Shea SM, Deshpande VS, Chung YC, Li D. Three-dimensional true-FISP imaging of the coronary arteries: improved contrast with T2-preparation. J Magn Reson Imaging 2002;15:597–602. [PubMed: 11997902]

26. Nehrke K, Bornert P, Manke D, Bock JC. Free-breathing cardiac MR imaging: study of implications of respiratory motion—initial results. Radiology 2001;220:810–815. [PubMed: 11526286]

27. Danias PG, Stuber M, Botnar RM, Kissinger KV, Edelman RR, Manning WJ. Relationship between motion of coronary arteries and diaphragm during free breathing: lessons from real-time MR imaging. AJR Am J Roentgenol 1999;172:1061–1065. [PubMed: 10587147]

28. Lai, P.; Larson, AC.; Nielles-Vallespin, S.; Li, D. Feasibility study of a double self-gating technique for free-breathing time-resolved 3D imaging. Proceedings of the 14th Annual Meeting of ISMRM; Seattle, USA. 2006. p. 1972

29. Manke D, Nehrke K, Bornert P, Rosch P, Dossel O. Respiratory motion in coronary magnetic resonance angiography: a comparison of different motion models. J Magn Reson Imaging 2002;15:661–671. [PubMed: 12112516]

30. Du YP, McVeigh ER, Bluemke DA, Silber HA, Foo TK. A comparison of prospective and retrospective respiratory navigator gating in 3D MR coronary angiography. The international journal of cardiovascular imaging 2001;17:287–294. discussion 295–286. [PubMed: 11599868]

31. Derbyshire JA, Herzka DA, McVeigh ER. S5FP: spectrally selective suppression with steady state free precession. Magn Reson Med 2005;54:918–928. [PubMed: 16155880]

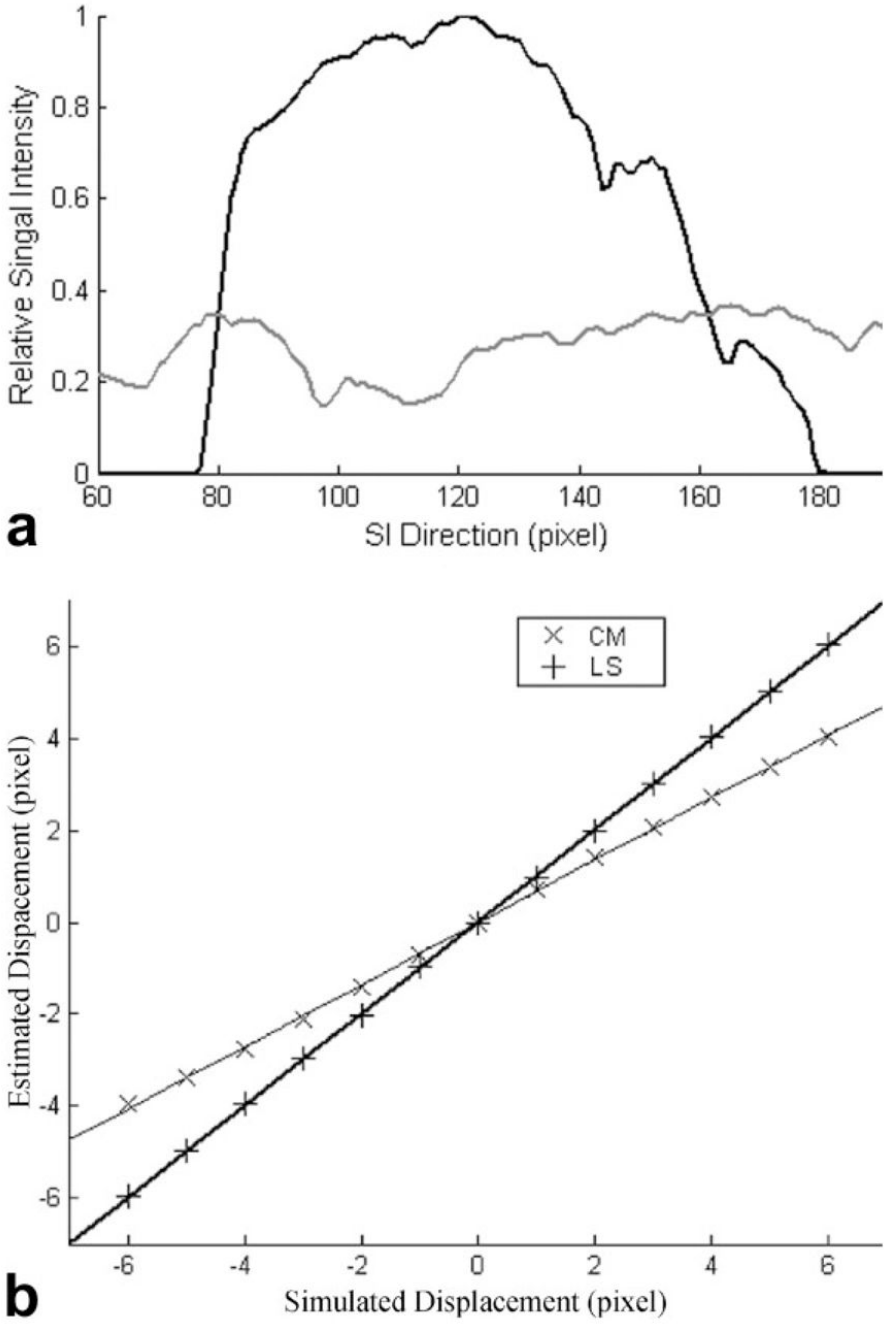

FIG. 1.

Simulation of the effects of anterior chest wall signal on target position estimation. **a:** The profiles of the simulated heart projection (dark) and the simulated anterior chest wall projection (gray). **b:** The target displacements in pixels (unit: 1.2 mm) estimated using CM and LS versus the simulated respiratory motion. The gray line ($y = 0.676 \times +5.500 \times 10^{-5}$) and the dark line ($y = 0.998 \times +0.154$) represent the linear regression lines fitted to the displacements derived using CM and LS, respectively.

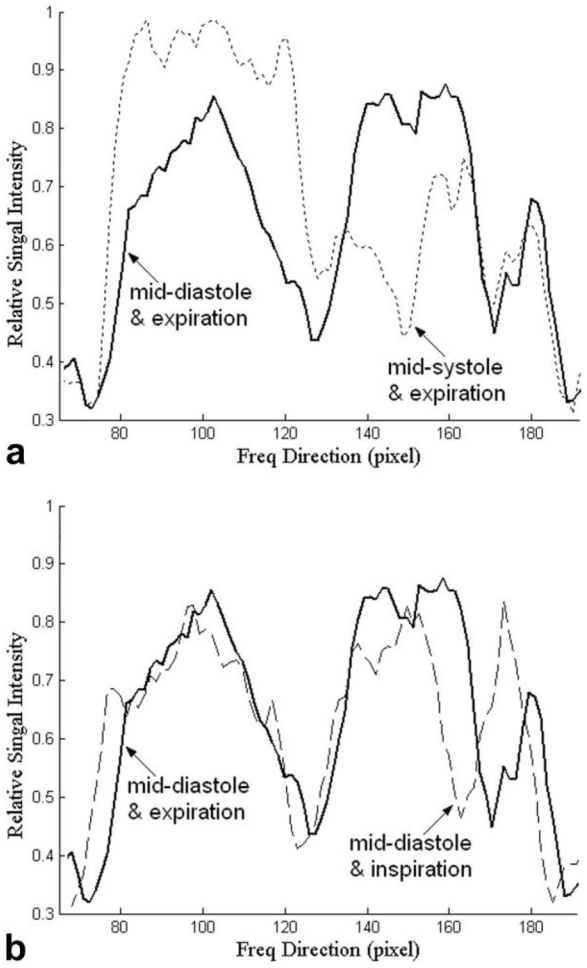

FIG. 2.
Variations of the projection profile due to cardiac motion (**a**) and respiratory motion (**b**).

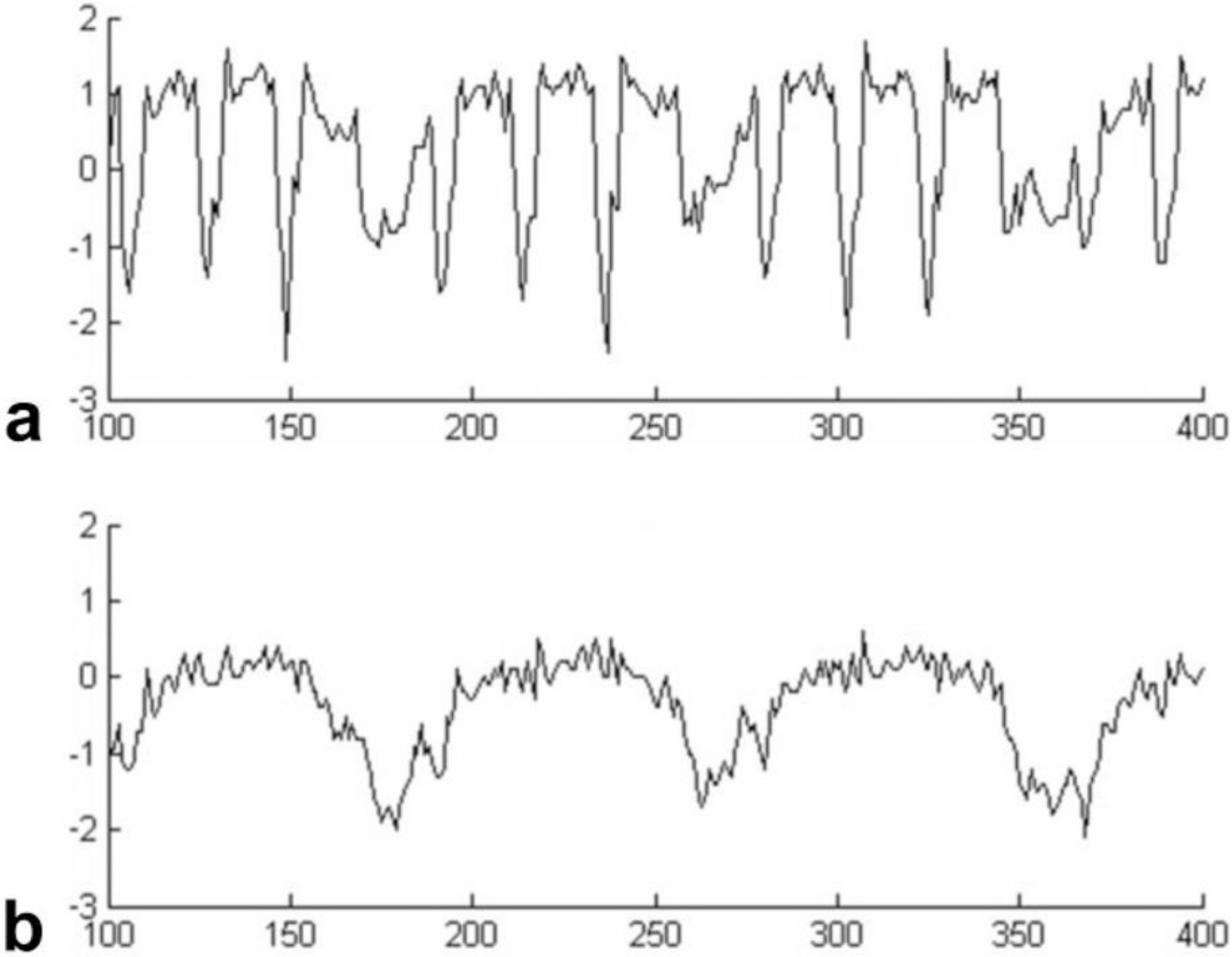

FIG. 3.

RSG profile shifts in the number of pixels (*y* axes) derived using the LS method with a single-phase template (**a**) and phase-specific templates (**b**). The *x* axes indicate the index of the acquired RSG projections and the time interval between two successive RSG projections is 51.6 ms. Notice that the signal in (a) is corrupted by cardiac motion while the signal in (b) shows a clear respiratory motion pattern.

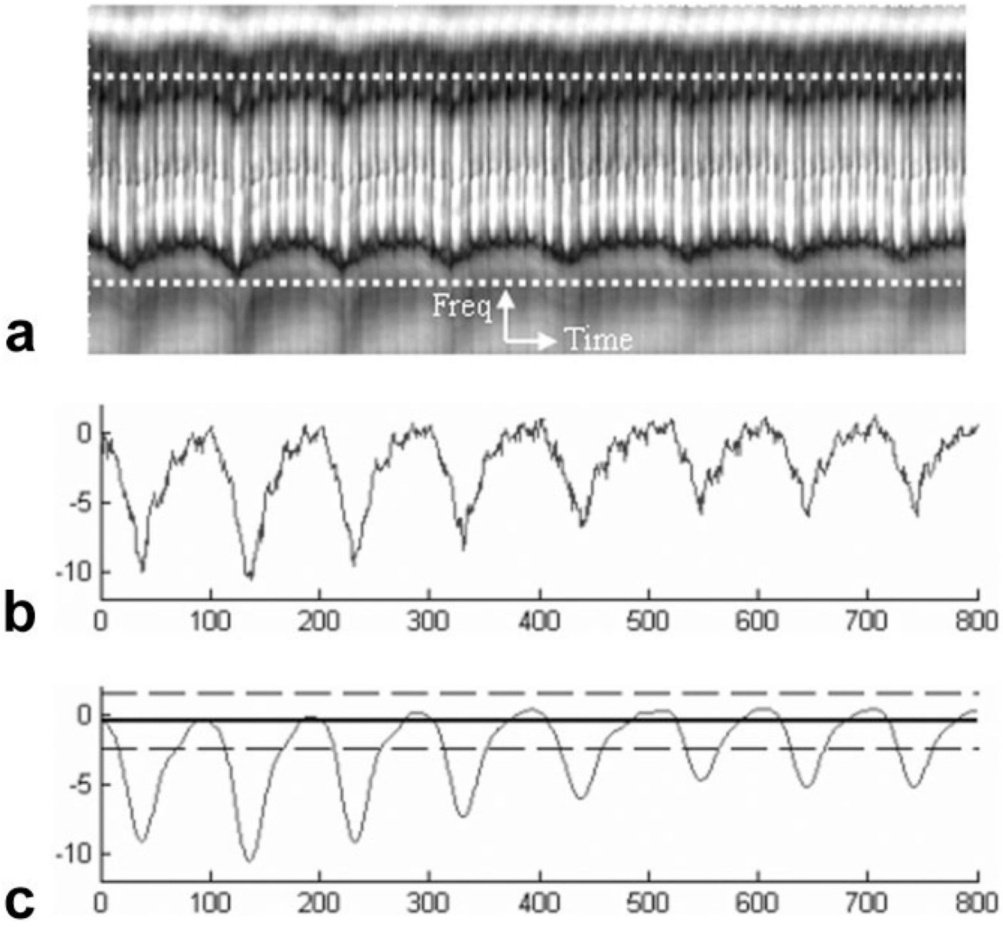

FIG. 4.

a: A segment of the time-series plot of the RSG projection. The dotted lines represent the upper and lower boundaries of the target region. **b:** The profile shift signal derived using LS. **c:** The corresponding RSG signal representing the breathing-induced target displacement after low-pass filtering. The solid bold line represents the RSG position and the two dashed lines represent the upper and lower boundaries of the GW. In (b) and (c), the *y* axes (unit: 1.0 mm) indicate the derived target position and the x axes (unit: 52.0 ms) indicate the RSG projection index.

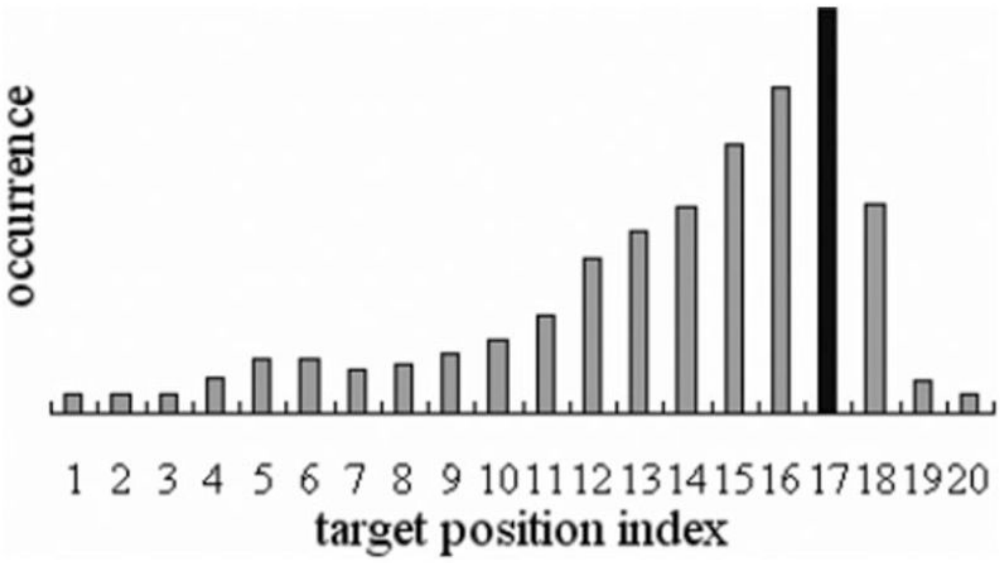

FIG. 5.
Determination of the RSG position. The position corresponding to the index with the most frequent occurrence was indicated by the black bar.

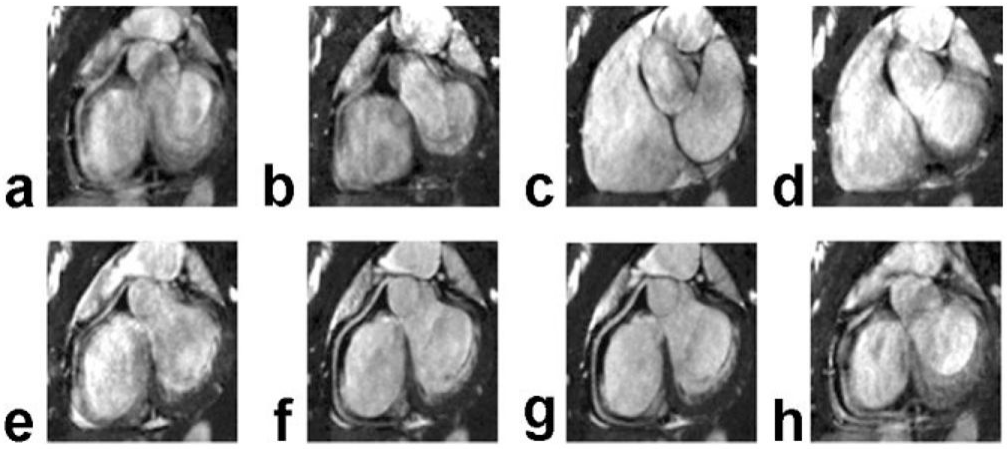

FIG. 6.

a– h: MIP images acquired using 4D RSG at cardiac phase 1, 3, 5, 7, 9, 11, 13, and 15, respectively.

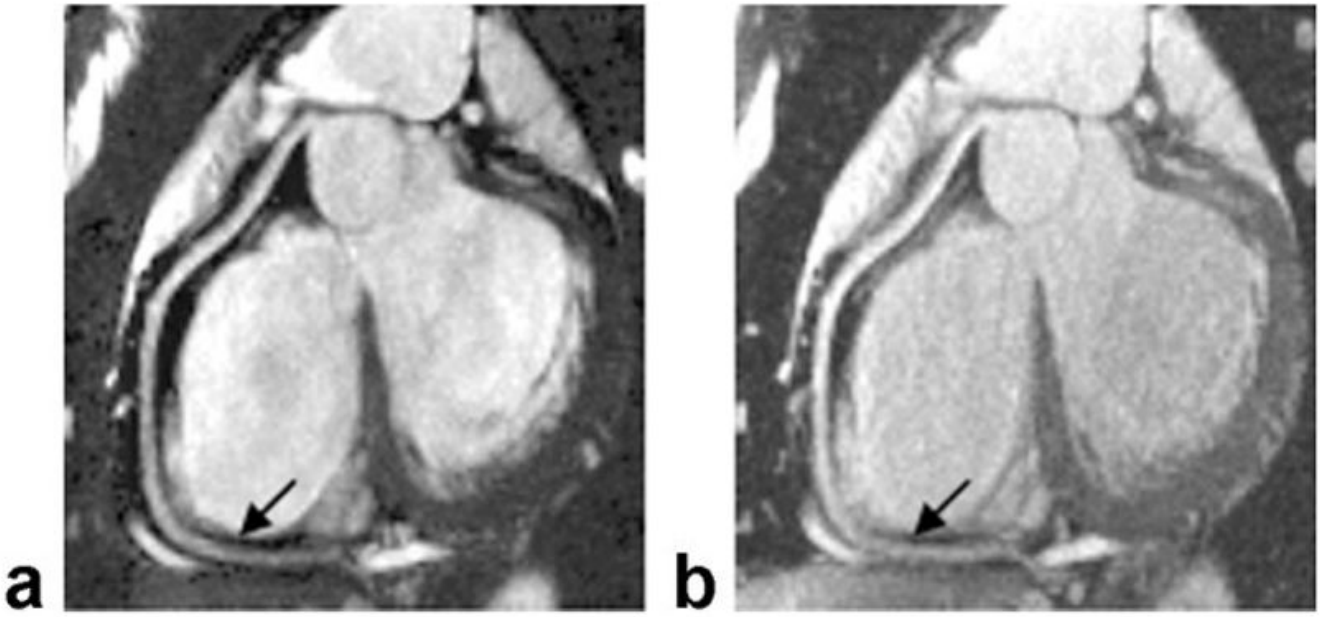

FIG. 7.
The mid-diastolic frame (cardiac phase 12) identified from 4D RSG images and the image acquired at mid-diastole using NAV.

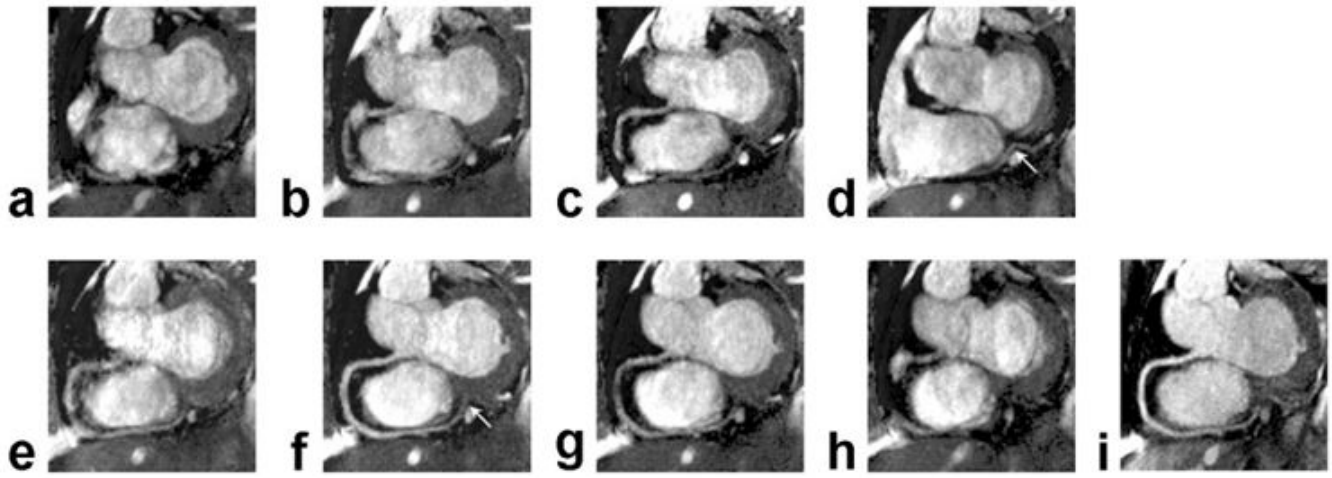

FIG. 8.

a– h: The cardiac frames acquired using 4D RSG at phase 1, 3, 5, 7, 9, 11, 13, and 15, respectively. **i:** The mid-diastole image acquired using NAV.

Table 1

Scores of the images reconstructed using NAV and RSG

Reconstruction methods	Reviewer 1	Reviewer 2	Averaged
NAV	2.86 ± 0.48	3.21 ± 0.70	3.04 ± 0.55
RSG	2.91 ± 0.47	3.43 ± 0.45	3.17 ± 0.43